International Journal of Nanoelectronics and Materials
IJNeaM
ISSN 1985-5761 | E-ISSN 2232-1535

# The potential of biographite formation from sago waste at different pyrolysis temperatures

Nurjehan Faratul Sabrina Kamaruddin [a], Siti Kudnie Sahari [a,b] *, Ibrahim Yakub [c], Marini Sawawi [d], Mohamad Rusop Mahmood [e], Ramzan Bin Mat Ayub [f], Zainab binti Ngaini [g], Yanuar Zulardiansyah Arief [a], Lilik Hasanah [h], and Rafeah binti Wahi [g]

[a]*Department of Electrical and Electronics Engineering, Faculty of Engineering, Universiti Malaysia Sarawak, 94300 Kota Samarahan, Sarawak, Malaysia*
[b]*Institute of Sustainable & Renewable Energy, Universiti Malaysia Sarawak 94300 Kota Samarahan, Sarawak, Malaysia*
[c]*Department of Chemical Engineering and Energy Sustainability, Universiti Malaysia Sarawak, 94300 Kota Samarahan, Sarawak, Malaysia*
[d]*Department of Mechanical and Manufacturing Engineering, Faculty of Engineering, Universiti Malaysia Sarawak, 94300 Kota Samarahan, Sarawak, Malaysia*
[e]*NANO-SciTech Centre, Universiti Teknologi Mara, Shah Alam, Selangor, Malaysia*
[f]*Institute of Nano Electronic Engineering, Universiti Malaysia Perlis, Kangar, Perlis, Malaysia*
[g]*Faculty of Resources Science and Technology, Universiti Malaysia Sarawak, 94300 Kota Samarahan, Sarawak, Malaysia*
[h]*Faculty of Mathematics and Sciences Education, Indonesia University of Education*
** Corresponding author. Tel.: +60-8258100; fax: +6082-583410; e-mail: sskudnie@unimas.my*

Received 09 May 2025, Revised 02 July 2023, Accepted10 July 2025

**ABSTRACT**

This study explores the potential of sago palm trunk as a precursor for synthesizing biographite for fuel cell applications. Pyrolysis was conducted at 500°C, 600°C, and 700°C, both in the presence and absence of iron (III) nitrate nonahydrate as a catalyst. The primary objective is to form biographite through pyrolysis at low heating temperatures. All samples were characterized by using scanning electron microscopy (SEM), Fourier transform infrared spectroscopy (FTIR), and a 3D digital microscope. Only the catalyst-treated samples were further analysed using X-ray diffraction (XRD) and Raman spectroscopy. To evaluate fuel cell performance, microbial fuel cells (MFCs) were constructed using the samples as bipolar plates. Results suggest that amorphous graphite can form at 500°C without a catalyst, whereas catalytic pyrolysis leads to the formation of nanocrystalline graphite. Among all tested samples, the catalyst-assisted pyrolysis at 600°C demonstrated the best fuel cell performance. These findings confirm the potential of the sago palm trunk for biographite synthesis. However, further optimization of the pyrolysis process beyond temperature control is needed to obtain crystalline graphite with enhanced electrical properties.

**Keywords:** *Biographite, Biomass, Microbial fuel cell, Pyrolysis, Sago palm trunk*

## 1. INTRODUCTION

As the world shifts towards renewable and more eco-friendly technologies, the need for sustainable materials such as carbon-rich substances made from biomass has drawn attention [1]. Coal-derived graphite, a widely used carbon-based material, poses significant environmental concerns. This includes greenhouse gas emissions and degradation of ecology during mining, which eventually limits the natural graphite stock [2]. Biographite, a carbon material synthesized from organic biomass such as agricultural waste, offers a renewable alternative for components in lithium-ion batteries, which are commonly used in electric vehicles (EVs) [3]. With EVs becoming more common, the reliance on conventional graphite should be lessened by focusing on the renewable choice.

Biographite has the ability to exhibit properties that are comparable to coal-derived graphite, such as electrical conductivity and chemical stability. Previous studies have successfully demonstrated the synthesis of biographite from various biomass sources, including lignin [4], bamboo [5], palm kernel shell (PKS) [6], oil palm trunk [7], and dandelion flower [8]. Bamboo, with over 70% lignocellulose, represents a valuable renewable resource for biomass-based applications [9]. Likewise, palm kernel shell (PKS), which has around 50% of lignin, has demonstrated significant potential for lignin extraction, which is crucial for making high-quality biographite [10]. Among these, dandelion flower stems are particularly notable due to their natural tubular structure, which enhances ion absorption and transport while maintaining high mechanical strength, low structural distortion, and an open-pore structure [8]. These features highlight the potential of dandelion-based as a sustainable feedstock for biographite production and green technologies.

Despite this, there are still plenty of obstacles in the synthesis process of biographite, especially in reaching material quality consistency and scalability. Variations in biomass type, pyrolysis conditions, and graphitization methods often lead to incompatible properties, such as low crystallinity and conductivity. Additionally, optimizing synthesis parameters, such as temperature, atmosphere,

and catalyst usage, remains complex and sometimes costly. These issues underline the need for further research to refine the graphitization process and explore new biomass sources with high carbon yields, as well as the desired characteristics for biographite production.

This study investigates the potential of sago palm trunk as a precursor for biographite synthesis, with a focus on its structural, thermal, and electrical characteristics. The ability to serve as an environmentally friendly alternative to graphite derived from coal is the primary goal of the study. This can be useful for the industry, such as lithium-ion batteries for electric vehicles, where they use graphite as part of their materials. By using several characterization techniques such as X-ray diffraction (XRD), Raman spectroscopy, and Fourier Transform Infrared Spectroscopy (FTIR), this study will explore the optimization of the synthesis process to ensure high material quality and performance. To the best of our knowledge, this is the first systematic study to evaluate sago palm trunk for biographite production, offering a new route to enhance biomass utilization in clean energy applications.

## 2. METHODOLOGY

### 2.1. Catalytic Pyrolysis of Sago Palm Trunk

The sago palm trunk was cut and diced into smaller pieces after being air-dried for 24 hours to remove moisture. The diced sago palm trunk was then heated at 70°C in an oven for a day. At room temperature, iron (III) nitrate nonahydrate was then dissolved in 100 mL of deionized water. The sago palm trunk sample from the oven was then stirred with a glass rod for an hour while submerged in the aqueous solution of iron (III) nitrate nonahydrate. For samples without a catalyst, the submersion step was skipped. After filtration, the sample was then dried at 85°C. For graphitization and pyrolysis, the sample was divided into three sections and heated to 500°C, 600°C, and 700°C, respectively. The sample was placed into a tube furnace and heated in a nitrogen environment for 8 hours. After the graphitization process, the remaining metal catalyst on the samples was washed with deionized water and stirred in hydrochloric acid for 30 minutes. Finally, the sample was dried overnight at 85°C in an oven.

Characterization of the samples was conducted using several techniques. Firstly, Fourier Transform Infrared Spectroscopy (FTIR) was used to identify functional groups in the samples for graphite formation confirmation. Secondly, Scanning Electron Microscopy-Energy Dispersive X-ray (SEM-EDX) was used to examine the surface morphology and element detection in the samples. Thirdly, a 3D digital microscope provided macroscopic observations of the texture and colour of the samples. Fourthly, Raman spectroscopy analysis was performed to assess the degree of graphitization by analysing the D and G bands. Last but not least, X-Ray Diffraction (XRD) was conducted to determine the crystalline structure and phase composition of the samples.

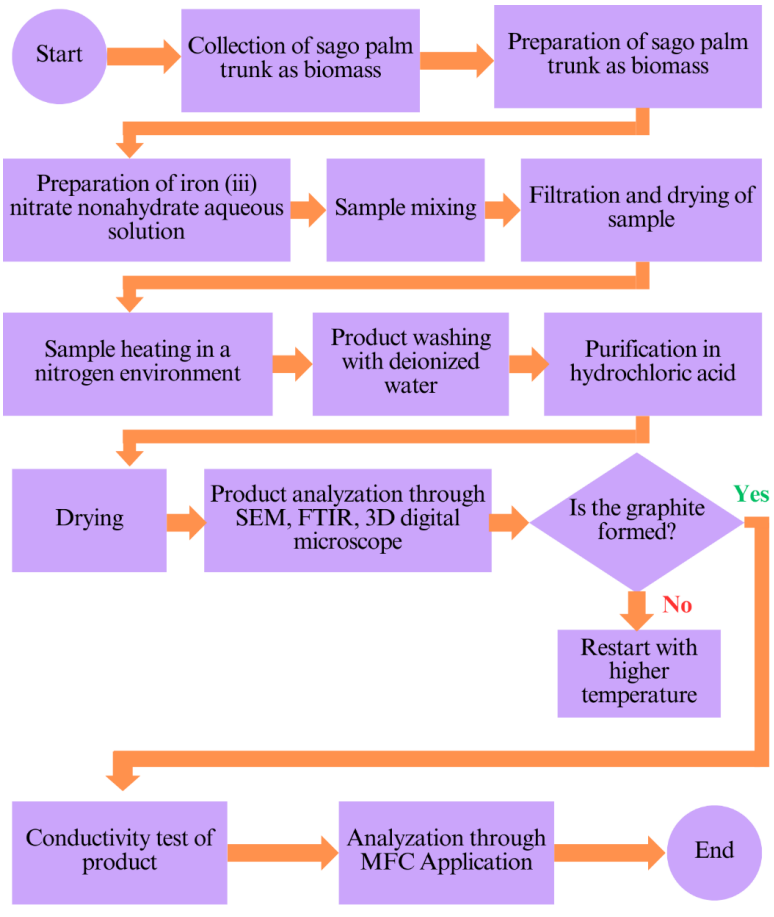


**Figure 1**. Catalytic pyrolysis of sago palm trunk flowchart


**Figure 2**. The pyrolysis process of sago palm trunk with $Fe(NO_3)_3 \cdot 9\ H_2O$ catalyst

### 2.2. Conductivity Test

The samples were tested using a multimeter in conductance mode. The produced graphite was directly tested by placing the probes on the samples. All the readings were recorded in the table.

### 2.3. Graphite Produced for MFC Application

To build an MFC, the samples formed from pyrolysis were crushed into powder. Steel mesh was cut into 3 × 3 cm pieces. Resin and hardener were mixed to glue the powder onto the steel mesh. Stripped wires were coiled and glued to the steel mesh, serving as the anode (red wire) and cathode (black wire) for the cell. Pond soil was used as the substrate, and both the anode and cathode were submerged in the soil. The constructed MFC was left for 15 hours to allow microorganisms to colonize the anode. All readings for the voltage and current of the open-circuit system were recorded.

The results from these analyses were compared across the different pyrolysis temperatures and between samples produced with and without the catalyst. The influence of temperature and catalyst on the degree of graphitization, structural properties, and functional groups was systematically evaluated. The catalytic effect of iron (III) nitrate nonahydrate was specifically assessed by comparing the quality of catalyst-treated samples to those synthesized without a catalyst. This methodology aimed to identify the optimal synthesis conditions for producing high-quality biographite from sago palm trunk, contributing valuable insights into the development of renewable materials for industrial applications.


**Figure 3**. MFC construction for all samples

## 3. RESULTS AND DISCUSSION

### 3.1. 3D Digital Microscope Analysis

Figure 4 presents the physical characteristics of the samples as observed using a 3D digital microscope with a 200 µm magnification scale. Under illumination, all samples exhibited notable reflectivity and a lustrous surface appearance. The products exhibited a soft texture and a uniform black colouration. No significant characteristic differences were observed between the catalytic and non-catalytic samples. In comparison to pure graphite, the analysed samples exhibited characteristic traits of graphite, including a smooth, glossy, and shiny surface, as well as a soft consistency [11]. These results imply that graphite-like properties are present in the samples. To further validate their structural and morphological properties, SEM analysis was conducted as in section 3.2. All the close-up views of the samples (1 mm) can be seen in Figure 5. Based on the results, the structure of all samples is edgy and non-flake shape. If compared to Figure 6, the structures are closer to amorphous and synthetic types of graphite rather than crystalline graphite, which has a clearer flake-shaped structure. SEM-EDX analysis is carried out to determine the product of the samples further.

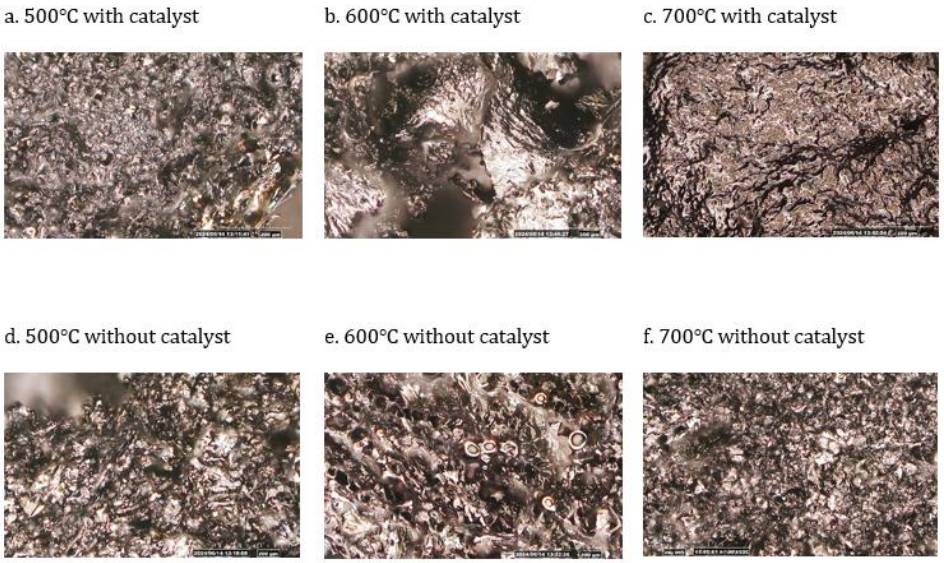


**Figure 4**. Surface of the samples through 3D-digital microscope

### 3.2. SEM Analysis

All the close-ups of the samples (1 mm) can be seen in Figure 5. Based on the results, the structure of all samples is edgy and non-flake shape. If compared to Figure 6, the structures are closer to amorphous and synthetic types of graphite rather than crystalline graphite, which has a clearer flake-shaped structure. SEM-EDX analysis is carried out to determine the product of the samples further.

The carbon content at various pyrolysis temperatures is shown in Figure 7 and Table 1, highlighting the influence of the catalyst. At 500°C, the carbon content is 70.92% in the presence of a catalyst, compared to 70.15% in its absence. As the temperature increases to 600°C, the carbon content rises to 75.63% with the catalyst, whereas it remains lower at 71.21% without it. At 700°C, the carbon content reaches its highest values, measuring 78.34% with the catalyst and 78.13% without it. These results imply that, especially at high temperatures, the catalytic process improves carbon retention as catalysts aid in the stabilisation of carbon structures, which improves graphitization [12]. Notably, the sample treated at 700°C with a catalyst exhibits the highest carbon content. This outcome can be attributed to the elevated temperature during pyrolysis, which facilitates the stabilisation of carbon structures and enhances covalent bonding. While elements such as hydrogen, oxygen, chlorine, and nitrogen are likely byproducts of the pyrolysis and acid-washing processes, the presence of silicon and zirconium may be attributed to external impurities and contaminants. Given that the samples' carbon content is between 70 and 85%, these results imply that they display traits of amorphous graphite [13].

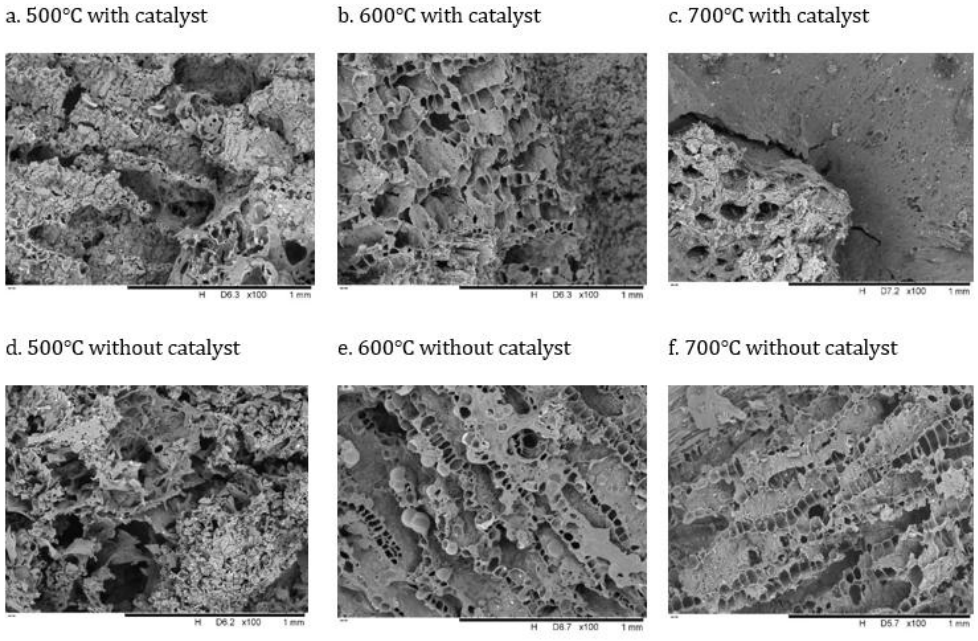


**Figure 5**. Structure of the samples through SEM analysis

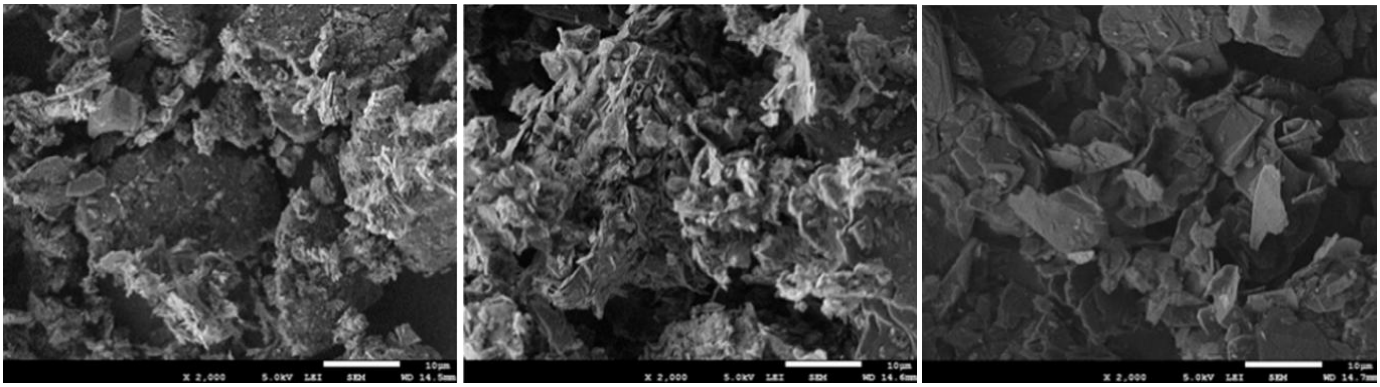

**Figure 6**. SEM analysis for amorphous, synthetic, and crystalline graphite's structure [14]

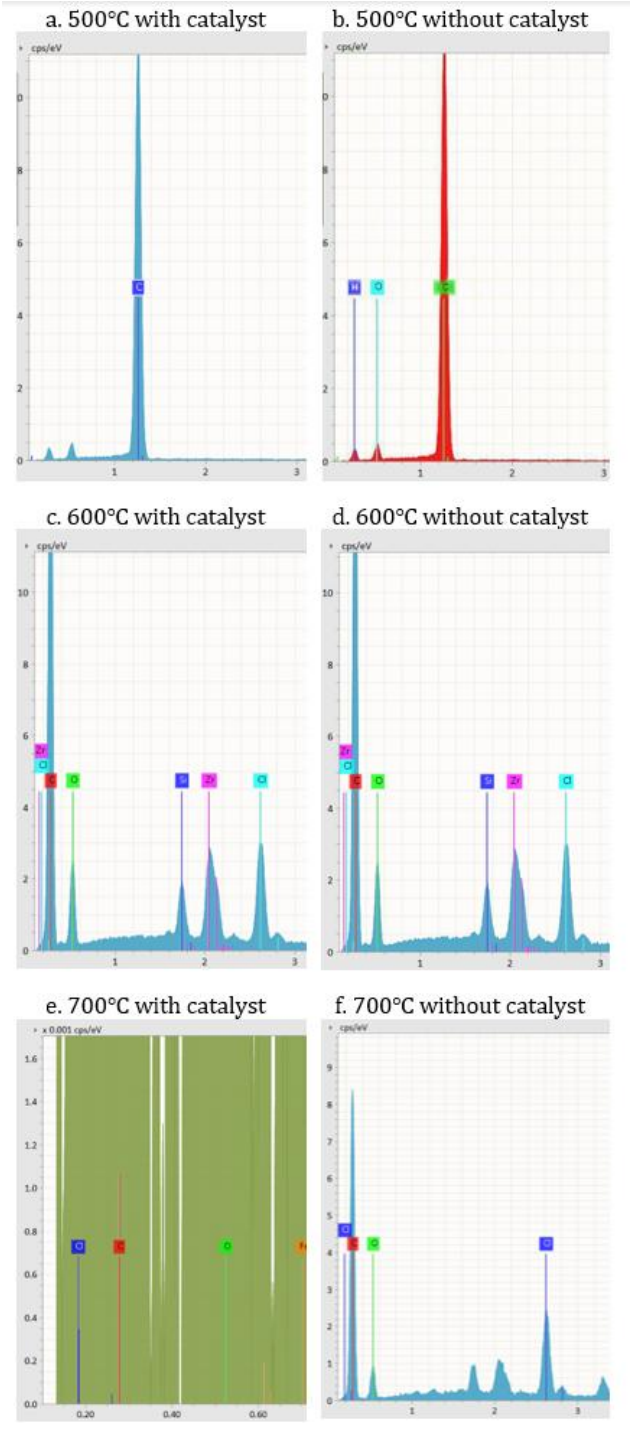


**Figure 7**. SEM-EDX result of the samples

**Table 1.** Carbon content, % for each sample from SEM-EDX analysis

| Temperature, T (°C) | Catalyst $Fe_3(NO_3)_3$ Presence | Carbon Content (%) |
|---|---|---|
| 500 | No | 70.15 |
| | Yes | 70.92 |
| 600 | No | 71.21 |
| | Yes | 75.63 |
| 700 | No | 78.13 |
| | Yes | 78.34 |

### 3.3. FTIR Test Analysis

The chemical composition and the molecular structure of the samples are analysed further through FTIR (Figure 8). For samples that have undergone pyrolysis at 500°C, the non-catalytic sample depicts three significant graphitic peaks, which are 1045 $cm^{-1}$, 3012.81 $cm^{-1}$, and 1620.21 $cm^{-1}$. This indicates C–O, C–H ($sp^2$) and C=C stretching exist in the sample. As for the catalytic sample, two significant peaks, 1037.7 $cm^{-1}$ and 1612.49 $cm^{-1}$ are detected. This suggests that C–O and C=C stretching exist too. A significant hybridised carbon ($sp^2$) of C–H shows contamination, impurities, or defects in the sample, suggesting that the catalytic sample is more favourable in this case [15, 16]. C-O stretching, however, indicates impurities and oxidation of the sample and this is also common even for natural graphite [16]. As for C=C stretching, also known as the G-band (graphite band), it is the most vital component to determine its graphitic structure. The peak intensity is a good indicator to determine it, as it shows the concentration of the bonds. A comparison of both samples reveals that the catalytic sample exhibits the highest concentration of C=C bonds (52.9%), whereas the non-catalytic sample shows the highest concentration of C-H bonds (64.8%), suggesting the defect in the graphitic structure in the non-catalytic sample is higher than that of the catalytic sample. For 500°C pyrolysis, it can be concluded that the catalytic sample is a better biographite than the non-catalytic sample.

In the case of samples pyrolyzed at 600°C, non-catalytic sample depicts four significant peaks and stretching which are 1053.13 $cm^{-1}$ (C–O), 2858.51 $cm^{-1}$ (C–H, $sp^3$), 3074.53 $cm^{-1}$ (C–H, $sp^2$), and 1616.35 $cm^{-1}$ (C=C)

meanwhile the catalytic sample shows five significant peaks and stretching, 1056.99 $cm^{-1}$ (C–O), 2924.09 $cm^{-1}$ (C–H, $sp^3$), 3005.1 $cm^{-1}$ (C–H, $sp^2$), 3093.82 $cm^{-1}$ (C–H, $sp^2$), and 1616.35 $cm^{-1}$ (C=C). As mentioned previously, the peak intensity serves as a reliable indicator for determination, as it reflects the concentration of the bonds. Both samples have the same stretching and it is noted that both also have the highest C–H ($sp^3$) concentration with 66.5% in the catalytic sample and 66.1% in the non-catalytic sample. In this case, the presence of $sp^3$ carbon in both samples, which are almost similar in concentration (%), disrupts the hexagonal carbon (graphite), exhibiting defects due to hydrogen [15, 16]. However, since C=C is the most prominent bond for graphitic structure determination, it is found that the concentration of C=C in the catalytic sample (58.6%) is higher than in the non-catalytic sample (56.6%). The catalytic sample is therefore a more effective biographite than the non-catalytic sample.

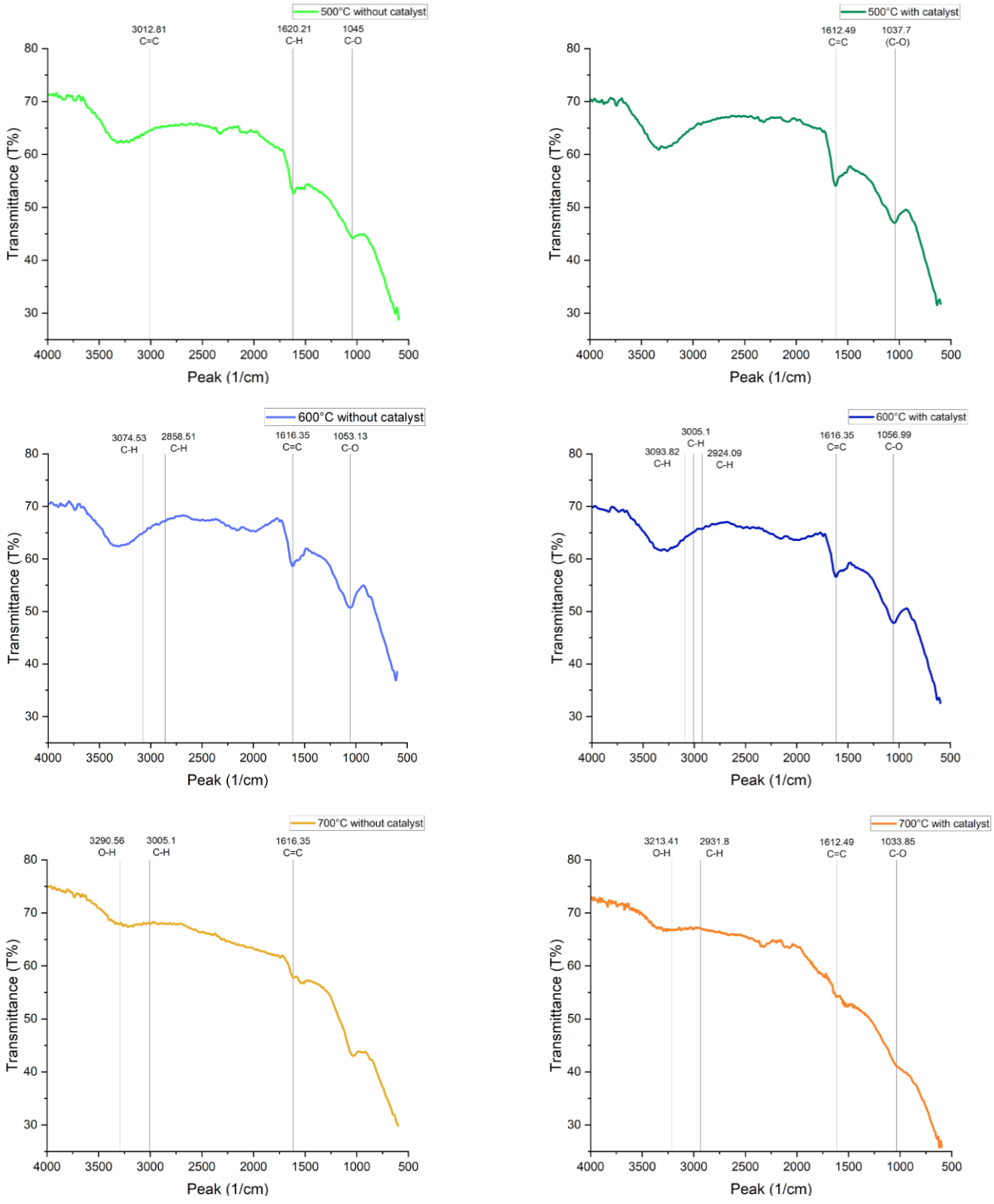


**Figure 8**. Carbon bonding that are detected in the samples through FTIR

**Table 2.** The presence of chemical bonds for each sample by FTIR

| Temperature, T (°C) | Catalyst $Fe_3(NO_3)_3$ Presence | Detected Peaks (1/cm) and Their Chemical Bonds |
|---|---|---|
| 500 | No | 1045.00 (C–O)<br>3012.81 (C–H)<br>1620.21 (C=C) |
| | Yes | 1037.70 (C–O)<br>1612.49 (C=C) |
| 600 | No | 1053.13 (C–O)<br>2858.51 (C–H)<br>3074.53 (C–H)<br>1616.35 (C=C) |
| | Yes | 1056.99 (C–O)<br>2924.09 (C–H)<br>3005.10 (C–H)<br>3093.82 (C–H)<br>1616.35 (C=C) |
| 700 | No | 3290.56 (O–H)<br>3005.10 (C–H)<br>1616.35 (C=C) |
| | Yes | 1033.85 (C–O)<br>2931.80 (C–H)<br>3213.41 (O–H)<br>1612.49 (C=C) |

For samples subjected to pyrolysis at 700°C, three significant peaks and stretching which are 3290.56 $cm^{-1}$ (O–H), 3005.1 $cm^{-1}$ (C–H, $sp^2$), and 1616.35 $cm^{-1}$ (C=C) are depicted in non-catalytic sample meanwhile four significant peaks for the catalytic sample, 1033.85 $cm^{-1}$ (C–O), 2931.8 $cm^{-1}$ (C–H, $sp^3$), 3213.41 $cm^{-1}$ (O–H), and 1612.49 $cm^{-1}$ (C=C). O–H stretching is the highest for both samples, showing moisture or hydroxyl groups mainly due to the acid washing with HCl, as it may emerge as a result of reactants implicated in the process (such as sulphuric acid, nitric acid, and formic acid) interacting with graphite [17]. This also indicates that the samples possess a large surface area and the ability to absorb atmospheric water which means they are likely amorphous or nanostructured [17]. When comparing C=C concentration, the catalytic sample exhibits a higher concentration at 57.7% compared to 54.1% in the non-catalytic sample. In comparison to the non-catalytic sample, the catalytic sample is a more efficient form of biographite.

An FTIR test is also conducted on a pure graphite electrode that was crushed into powder form. In Figure 9, the FTIR graph from the pure graphite can be seen having the same ranges when compared with the other six samples. The peaks are ranging around 1640–3200 $cm^{-1}$. Pure graphite illustrates fewer peaks since it does not have any contamination or reactant. Based on this comparison, it can be said that the product produced is highly graphite. Not just because of the presence of carbon elements, but also because C=C in the samples is detected, which shows the graphite bonding.

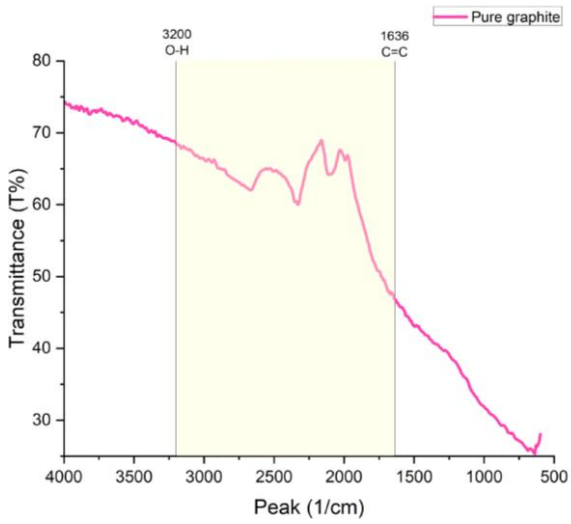


**Figure 9**. FTIR range of pure graphite

### 3.4. Raman Spectroscopy Analysis

The analysis of the catalysed samples is further characterised via Raman spectroscopy. Figure 10 shows that pure graphite exhibits a subtle peak at 1343 $cm^{-1}$, a sharp peak at 1586 $cm^{-1}$, and a 2D band at 2684 $cm^{-1}$. In contrast, the catalysed samples display peaks at 1357 $cm^{-1}$ and 1593 $cm^{-1}$ (500°C), 1353 $cm^{-1}$ and 1594 $cm^{-1}$ (600°C), and 1387 $cm^{-1}$ and 1604 $cm^{-1}$ (700°C). These peaks suggest the possible presence of C=C bonds, while the C–H bond is additionally detected in pure graphite. The 2D band, also known as the G' band, results from the convolution of multiple peaks in graphite [18, 19]. The broadening and shifting of this band in the catalyzed samples indicate structural disorder or stacking defects, whereas the sharp and intense peak in pure graphite reflects a well-ordered structure.

The degree of structural disorder or defect density in graphitic materials can be inferred from the intensity of the D band. Since the D band arises from a double resonance process, its intensity is highly sensitive to the presence of defects, vacancies, and impurities within the material [18]. This band typically appears at approximately 1360 $cm^{-1}$, serving as a key indicator of disorder in graphitic structures. However, in this experiment, peak position is a more reliable parameter than intensity for material identification and differentiation. All samples exhibit the D band (~1343–1357 $cm^{-1}$) and G band (~1586–1604 $cm^{-1}$), which are indicative of graphitic structures with different levels of disorder. The 2D band (~2684 $cm^{-1}$) is clearly visible in the pure graphite sample but becomes weaker or shifts in the catalyzed samples, suggesting structural changes [18, 19]. The peak positions of the catalyzed samples show a minor shift, suggesting bonding modifications or strain effects [18, 19].

In Figure 11, with pure graphite (black line) as the reference peak, the 600°C sample (green line) has a G band peak position closest to pure graphite and a relatively consistent shape, while the 500°C sample (red line) has an intense D band, suggesting more defects, likely due to defect introduction during catalytic treatment. The 700°C sample

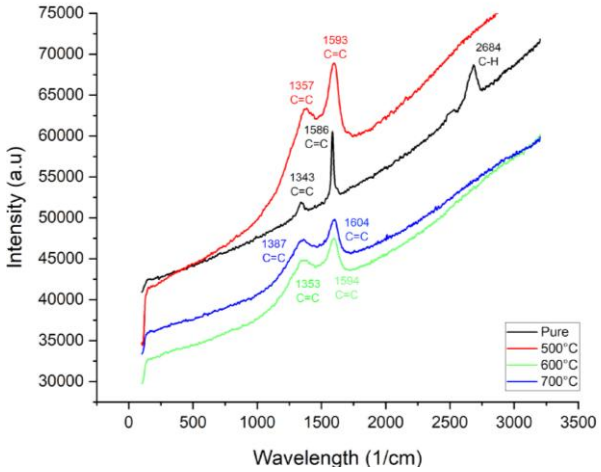


**Figure 10**. The Raman Spectroscopy graphs for the pure graphite and the samples

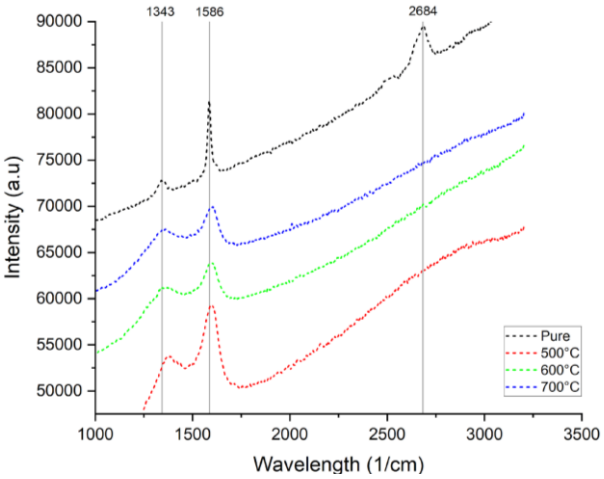


**Figure 11**. Peak positions of the samples compared to pure graphite

(blue line) shows peak broadening, indicating excessive structural degradation or increased amorphization [18]. Because the 600°C sample's G band is closest to that of pure graphite and it retains a comparatively well-defined structure with less broadening than the 700°C sample, it may be concluded from the data that this sample is the most structurally advantageous.

Furthermore, the absence of a distinct 2D band, coupled with the presence of the G band, suggests that the samples are likely composed of nanocrystalline graphite rather than highly ordered graphitic structures, as shown in Figure 12 [20]. This is characteristic of disordered carbon materials, where the reduction in long-range order suppresses the formation of a well-defined 2D band. Additionally, the broadening of peaks, rather than the sharp features typically observed in crystalline graphite, further supports the amorphous nature of the samples [20]. These findings highlight the influence of synthesis conditions on the structural evolution of graphitic materials, emphasizing the transition from ordered to nanocrystalline or amorphous phases.

### 3.5. XRD Analysis

Given that the catalytic samples exhibit a more well-defined graphitic structure, they were further analysed using XRD. For reference, the pure graphite sample, as illustrated in Figure 13, presents a prominent peak at 2θ = 26.628° with a corresponding d-spacing of 3.35 Å, along with secondary peaks at 2θ = 42.465°, 54.754°, 77.555°, 83.684°, and 87.123°, corresponding to d-spacings of 2.13 Å, 1.68 Å, 1.23 Å, 1.12 Å, and 1.12 Å, respectively. For the pyrolyzed samples, the XRD patterns reveal distinct peaks that vary with temperature. At 500°C, diffraction peaks are observed at 2θ = 28.451° and 40.662°, with d-spacings of 3.13 Å and 2.21 Å, respectively. The d-spacings at 600°C are 3.14 Å, 2.22 Å, 1.57 Å, 1.21 Å, and 1.19 Å, respectively, with the additional peaks appearing at 2θ = 28.386°, 40.591°, 58.703°, 78.715°, and 80.364°. Finally, at 700°C, the peaks are identified at 2θ = 28.444° and 40.638°, with d-spacings of 3.14 Å and 2.21 Å, respectively.

The diffraction line widths of the (002) and (100) reflections are typically examined in order to confirm the

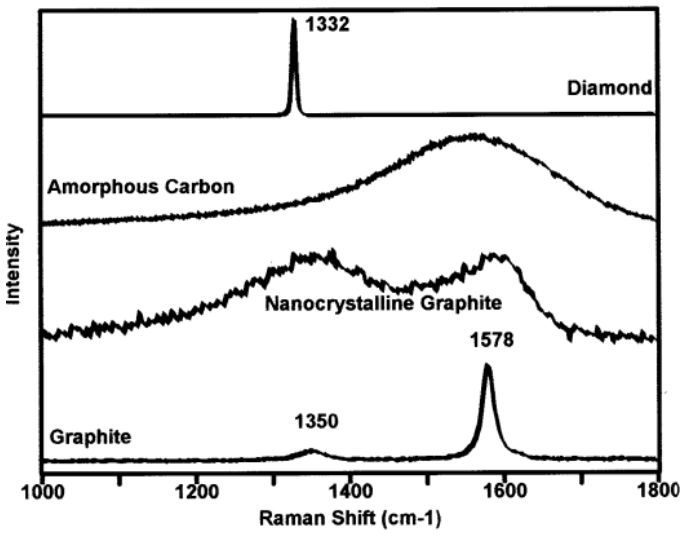


**Figure 12**. Raman spectroscopy of nanocrystalline graphite [20]

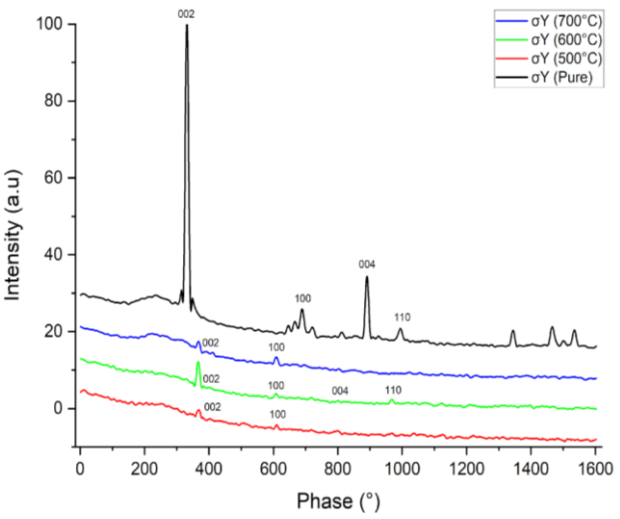


**Figure 13**. XRD graphs for pure graphite and the catalyzed samples

crystallite sizes of graphite along different crystallographic axes [21]. The XRD analysis depicts multiple planes, including (002), (004), (100), and (110), which align with the characteristics of graphite. Nevertheless, the different temperatures of the pyrolyzed samples show different degrees of structural order. Specifically, for the samples pyrolyzed at 500°C and 700°C, they display only the (002) and (100) reflections, meaning a less complete graphitization process. On the other hand, the sample underwent pyrolysis at 600°C, successfully showing the same diffraction planes as pure graphite, including (002), (004), (100), and (110), but with lower intensity. This suggests that the graphitization process at 600°C is more effective in producing a well-ordered crystalline structure. The higher structural ordering recorded at 600°C may be the cause from ideal temperature that allows the rearrangement of carbon layers, promoting better crystallinity for the sample. The formation of a more prominent turbostratic graphite phase, which closely resembles the properties of natural graphite, is further supported by the presence of the (004) and (110) peaks [22, 23]. Turbostratic graphite shows partial graphitisation, which is not yet entirely crystalline but is more organized than amorphous carbon [22, 23]. These findings reveal that 600°C is the most favourable temperature for achieving structural order in the sago palm trunk pyrolysis.

In addition, as shown in the accompanying figure, the samples also depict significantly lower peak intensities than pure graphite. The reduction in peak intensity indicates a lower degree of crystallographic orientation within the sample [24]. Among the samples, 600°C-sample shows the highest intensity. Furthermore, compared to pure graphite, the sample's diffraction peaks are substantially bigger. Smaller crystallite sizes and more structural disorder corresponded with these larger peaks [22]. These results imply that the samples had an amorphous or weakly crystalline graphite phase.

### 3.6. Conductivity Test

The purpose of the conductivity test is to compare the performance of the synthesised products with that of pure graphite and assess their electrical conductivity. The sample synthesized with a catalyst at 600°C exhibited the highest conductivity, measured at 1124 S/cm, as shown in Table 3.

For comparison, pure graphite typically has a conductivity range of 500–1700 S/cm [25]. According to the results, the samples produced using a catalyst at 600°C and 700°C have conductivity values that are comparable to those of pure graphite, implying their great potential for electrical applications. This outcome aligns with earlier characterization results, where the 600°C catalyzed sample exhibited the most developed graphitic structure and distinct nanocrystalline graphite features. Additionally, these results suggest the presence of a catalyst continuously improves conductivity, most likely as a result of its ability to promote structural ordering and lessen imperfections in the carbon matrix [12].

### 3.7. MFC Analysis

#### 3.7.1. Voltage Readings of MFC Samples for a Week

The highest recorded voltage was 0.641V, observed in the 600°C catalysed sample, whereas the lowest was 0.026V, obtained from the 500°C non-catalysed sample. Over the course of a week, most samples exhibited a general increase in voltage, suggesting progressive microbial activity and electrode stability. However, the 500°C samples portrayed an initial increment followed by a decline, indicating instability in MFC application.

**Table 3.** Carbon content, % for each sample from SEM-EDX analysis

| Temperature, T (°C) | Catalyst $Fe_3(NO_3)_3$ Presence | Conductivity, G (S/cm) |
|---|---|---|
| 500 | No | 85 |
| | Yes | 308 |
| 600 | No | 206 |
| | Yes | 1124 |
| 700 | No | 180 |
| | Yes | 808 |

**Table 4.** Open circuit system voltage reading of MFC samples for a week

| Day | 500℃ No Catalyst (V/V) | 500℃ With Catalyst (V/V) | 600℃ No Catalyst (V/V) | 600℃ With Catalyst (V/V) | 700℃ No Catalyst (V/V) | 700℃ With Catalyst (V/V) |
|---|---|---|---|---|---|---|
| 1 | 0.026 | 0.177 | 0.027 | 0.325 | 0.038 | 0.166 |
| 2 | 0.191 | 0.372 | 0.052 | 0.354 | 0.057 | 0.132 |
| 3 | 0.213 | 0.351 | 0.043 | 0.361 | 0.076 | 0.137 |
| 4 | 0.242 | 0.336 | 0.072 | 0.411 | 0.089 | 0.144 |
| 5 | 0.198 | 0.331 | 0.094 | 0.423 | 0.093 | 0.138 |
| 6 | 0.253 | 0.325 | 0.088 | 0.514 | 0.094 | 0.221 |
| 7 | 0.286 | 0.283 | 0.119 | 0.641 | 0.115 | 0.231 |

As illustrated in Figure 14, the voltage trends for each sample are clearly distinguishable. The 600°C catalysed samples demonstrated a significant rise in voltage, highlighting their better performance. A similar trend was observed in the 700°C catalysed samples, albeit with slightly smaller values. Numerous parameters, such as soil humidity, the total surface area of the electrodes exposed to bacterial colonies, and the degree of bacterial growth on the electrode surfaces, might be attributed to the observed variances in performance [26]. Within the MFC system, these parameters have substantial effects on electron transfer efficiency and microbial interactions [26]. But in this instance, it is probably because catalysed samples, particularly when catalysed at 600°C, have stronger graphitic structures. The carbon structure of amorphous graphite in non-catalytic samples is more disordered compared to nanocrystalline graphite in catalytic samples due to the absence of long-range crystalline organization [27]. When exposed to oxidizing conditions, particularly at high temperatures, this instability accelerates degradation by introducing a large number of oxidation-prone active sites [27]. Over time, the material's electrical and structural integrity may be jeopardized by these active sites' growing reactivity [27].

Overall, the results underscore the potential of graphite-based electrodes for MFC applications, especially those synthesised via a catalyst at 600°C. Their potential as affordable and effective electrode materials for sustainable energy generation is suggested by their high conductivity, stability, and capacity to promote microbial electron transfer.

### 3.7.2. Current Readings of MFC Samples for a Week

As presented in Table 5, the current readings for all samples demonstrated a fluctuating trend, with an initial rise followed by a decline. This instability suggests that factors such as bacterial colonization efficiency and electrode surface interactions may influence the current output over time [26]. The fluctuations in these samples can be seen clearly in Figure 15, which illustrates the current trends for the microbial fuel cells (MFCs).

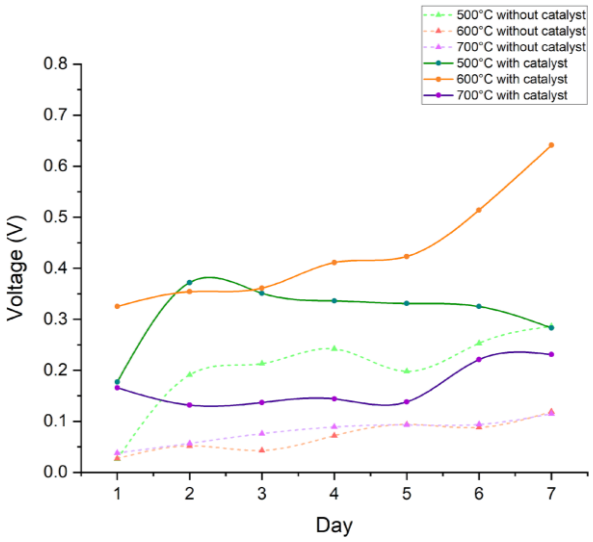


**Figure 14**. Voltage readings of MFCs for a week

In conjunction, the samples that were catalysed at 600°C mainly had the greatest current values, suggesting the catalyst's beneficial effects on boosting microbial activity and electron transfer. This improvement is attributable to the catalyst's function in strengthening the electrode material's electrical and structural characteristics, which promotes more efficient charge transport. Furthermore, the bacterial population in the system, which requires a particular amount of time to form a stable anodic biofilm, may have an effect on the observed fluctuations in current production [26]. Since this biofilm is the main interface between the bacteria and the electrode, its development and maturity are essential for long-term electron transmission [26].

These results add to the possibility of catalysed graphite electrodes for use in MFCs, especially those synthesised at 600°C. Its high conductivity and compatibility with microorganisms imply that it may be used as an affordable and efficient substitute for conventional electrode materials, promoting the creation of sustainable bioelectrochemical energy systems. Furthermore, the overall performance of MFCs indicates that nanocrystalline

**Table 5.** Open circuit system current reading of MFC samples for a week

| Day | 500℃ No Catalyst (I/μA) | 500℃ With Catalyst (I/μA) | 600℃ No Catalyst (I/μA) | 600℃ With Catalyst (I/μA) | 700℃ No Catalyst (I/μA) | 700℃ With Catalyst (I/μA) |
|---|---|---|---|---|---|---|
| 1 | 0.5 | 1.1 | 0.5 | 2.6 | 0.8 | 2.7 |
| 2 | 0.4 | 1.4 | 0.7 | 2.7 | 0.5 | 2.8 |
| 3 | 0.4 | 1.5 | 0.6 | 2.8 | 0.5 | 2.9 |
| 4 | 0.5 | 1.3 | 0.8 | 2.9 | 0.6 | 2.9 |
| 5 | 0.5 | 1.3 | 0.9 | 2.9 | 0.5 | 3.0 |
| 6 | 0.6 | 1.2 | 0.8 | 3.1 | 0.9 | 3.0 |
| 7 | 0.7 | 0.9 | 1.0 | 3.3 | 1.1 | 3.1 |

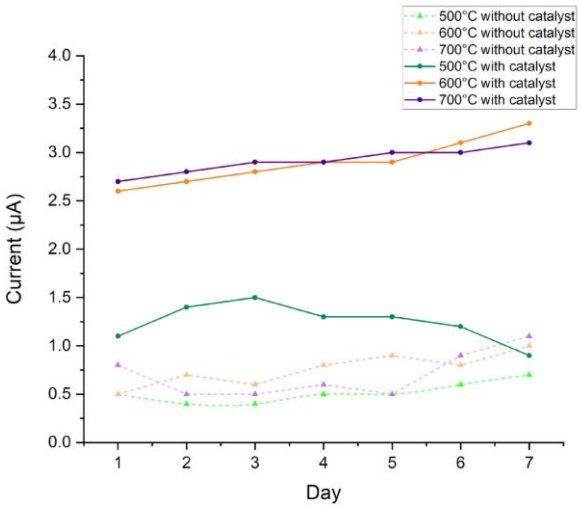


**Figure 15**. Current readings of MFCs for a week

graphite, obtained in catalyst samples, exhibits better long-term reliability and durability compared to amorphous graphite in non-catalytic samples. This enhanced performance can be attributed to its well-ordered crystalline structure, which facilitates better electrical conductivity, structural stability, and resistance to degradation over prolonged operating periods.

### 3.8. Ideal Samples

In short, an ideal sample may be varied depending on the use and its importance. For example, the sample synthesized at 500 °C without a catalyst is sufficient to form amorphous graphite. This lower-temperature, catalyst-free process is more environmentally friendly. The amorphous graphite formed can be used in lubricant additives, paints, and even pencils. However, in terms of fuel cell application, a sample that shows better electrical properties is more favoured which in this case is 600°C-with-catalyst-sample. Raman spectroscopy confirmed that all catalytic samples exhibit nanocrystalline graphite structures, with the 600 °C catalyzed sample showing peak positions closest to those of crystalline graphite. This is further supported by XRD analysis. Theoretically, the 700 °C sample that has the highest carbon content per SEM-EDX would be expected to exhibit the best electrical performance. However, factors such as surface functionalization, moisture adsorption, sample oxidation, and potential contamination during characterization may have influenced the observed results. To address these issues, future studies should consider higher graphitization temperatures (2000–3000 °C) or extended heat treatment durations to achieve better crystallinity. Additionally, improved sample handling and environmental control during synthesis and characterization are recommended.

## 4. CONCLUSION

This study highlights the potential for producing biographite from sago palm trunk. This investigation yielded several observations. First, at as low as 500°C temperature during pyrolysis, samples with no catalyst can form amorphous graphite. Second, samples that undergo pyrolysis with a catalyst depict higher conductivity, making them a better choice for fuel cell uses. In addition, all of the catalytic samples are confirmed to be nanocrystalline graphite, after further characterization via XRD and Raman spectroscopy. From the analysis, the 600°C-with-catalyst-sample suggests the best sample for MFCs application. Overall, these results demonstrate the potential of sago palm trunk for biographite formation and use in MFCs.

**Table 6.** Summary of the ideal results of all tests and analysis

| Test / Analysis | Ideal Sample | Remarks |
|---|---|---|
| 3D-digital microscope | 500°C without catalyst | • Sample shows graphite physical characteristics.<br>• Graphite is most likely to form under the lowest temperature with no additional chemical (catalyst) usage. |
| SEM | 700°C with catalyst | • Highest carbon content at 78.34%.<br>• Amorphous graphite is likely formed. |
| FTIR | 600°C with catalyst | • C=C stretching is successfully detected in the sample.<br>• The concentration of C=C bond is the highest.<br>• Catalyzed sample is a more effective biographite compared to non-catalyzed sample. |
| Raman spectroscopy | 600°C with catalyst | • Sample has the closest peak position to pure graphite.<br>• Sample has the most consistent graph pattern. |
| XRD | 600°C with catalyst | • Sample has the 2θ peaks range of crystalline graphite.<br>• Sample depicts the closest peaks position with crystalline graphite.<br>• Sample exhibits the same diffraction planes as pure graphite. |
| Conductivity | 600°C with catalyst | • Highest reading for conductivity at 1124 S/cm.<br>• Samples with catalyst has higher conductivity compared to samples without catalyst. |
| MFC application | 600°C with catalyst | • Highest with the most stable voltage and current readings for open circuit system. |

**ACKNOWLEDGMENTS**

This research was funded by Tun Openg Chair, grant, UNI/F02/TOC/85604/2023 and Universiti Malaysia Sarawak.

**REFERENCES**

[1] M. Zhang, J. Zhang, S. Ran, W. Sun, and Z. Zhu, "Biomass-Derived sustainable carbon materials in energy conversion and storage applications: Status and opportunities. A mini review," *Electrochemistry Communications*, vol. 138, p. 107283, 2022.

[2] Z. Shi *et al.*, "Establishment of green graphite industry: Graphite from biomass and its various applications," *SusMat*, vol. 3, no. 3, pp. 402–415, 2023.

[3] L. He *et al.*, "Research progress on high-rate graphite anode materials for lithium-ion batteries," *Journal of Energy Storage*, vol. 111, p. 115426, 2025.

[4] M. Demir *et al.*, "Graphitic Biocarbon from Metal-Catalyzed Hydrothermal Carbonization of Lignin," *Industrial & Engineering Chemistry Research*, vol. 54, no. 43, pp. 10731–10739, 2015.

[5] S. Xia *et al.*, "Fe–Co based synergistic catalytic graphitization of biomass: Influence of the catalyst type and the pyrolytic temperature," *Energy*, vol. 239, p. 122262, 2022.

[6] N. H. Jabarullah, A. S. Kamal, and R. Othman, "A Modification of Palm Waste Lignocellulosic Materials into Biographite Using Iron and Nickel Catalyst," *Processes*, vol. 9, no. 6, p. 1079, 2021.

[7] N. A. Karim, M. M. Ramli, C. M. R. Ghazali, C. A. I. Nadia, and G. Denesh, "Low temperature synthetic graphite from oil palm trunk waste via pyrolisis process," *IOP Conference Series: Materials Science and Engineering*, vol. 932, no. 1, p. 012125, 2020.

[8] Y. Tan, Z. Xu, L. He, and H. Li, "Three-dimensional high graphitic porous biomass carbon from dandelion flower activated by $K_2FeO_4$ for supercapacitor electrode," *Journal of Energy Storage*, vol. 52, p. 104889, 2022.

[9] Z. Liang, A. Neményi, G. P. Kovács, and C. Gyuricza, "Potential use of bamboo resources in energy value-added conversion technology and energy systems," *GCB Bioenergy*, vol. 15, no. 8, pp. 936–953, 2023.

[10] A. Boonsombuti, N. Phinichkha, S. Supansomboon, and A. Luengnaruemitchai, "The use of lignin from palm kernel shell (PKS) to fabricate oil palm mesocarp fiber (OPMF) particleboards," *International Journal of Adhesion and Adhesives*, vol. 125, p. 103425, 2023.

[11] S. Sabhadiya, "What are the main properties of graphite?," The Engineering Choice. https://www.theengineeringchoice.com/what-are-the-main-properties-of-graphite/

[12] M. Devi, S. Rawat, and S. Sharma, "A comprehensive review of the pyrolysis process: from carbon nanomaterial synthesis to waste treatment," *Oxford Open Materials Science*, vol. 1, no. 1, 2020.

[13] A. D. Jara, A. Betemariam, G. Woldetinsae, and J. Y. Kim, "Purification, application and current market trend of natural graphite: A review," *International Journal of Mining Science and Technology*, vol. 29, no. 5, pp. 671–689, 2019.

[14] Y. Rew, A. Baranikumar, A. V. Tamashausky, S. El-Tawil, and P. Park, "Electrical and mechanical properties of asphaltic composites containing carbon based fillers," *Construction and Building Materials*, vol. 135, pp. 394–404, 2017.

[15] C. H. Manoratne, S. R. D. Rosa, and I. R. M. Kottegoda, "XRD-HTA, UV Visible, FTIR and SEM Interpretation of Reduced Graphene Oxide Synthesized from High Purity Vein Graphite," *Material Science Research India*, vol. 14, no. 1, pp. 19–30, 2017.

[16] O. S. Papaianina *et al.*, "Graphite Oxide – Stages of Formation and a New View on Its Structure," *Theoretical and Experimental Chemistry*, vol. 49, no. 2, pp. 88–95, 2013.

[17] V. Ţucureanu, A. Matei, and A. M. Avram, "FTIR Spectroscopy for Carbon Family Study," *Critical Reviews in Analytical Chemistry*, vol. 46, no. 6, pp. 502–520, 2016.

[18] A. C. Ferrari, "Raman spectroscopy of graphene and graphite: Disorder, electron–phonon coupling, doping and nonadiabatic effects," *Solid State Communications*, vol. 143, no. 1–2, pp. 47–57, 2007.

[19] C. Sole, N. E. Drewett, and L. J. Hardwick, "*In situ* Raman study of lithium-ion intercalation into microcrystalline graphite," *Faraday Discuss.*, vol. 172, pp. 223–237, 2014.

[20] D. R. Tallant, T. A. Friedmann, N. A. Missert, M. P. Siegal, and J. P. Sullivan, "Raman Spectroscopy of Amorphous Carbon," *MRS Proceedings*, vol. 498, p. 37, 1997.

[21] A. Milev, M. Wilson, G. S. K. Kannangara, and N. Tran, "X-ray diffraction line profile analysis of nanocrystalline graphite," *Materials Chemistry and Physics*, vol. 111, no. 2–3, pp. 346–350, 2008.

[22] D. Andersson, A. Brunnberg, and E. Lind, "Catalytic Graphitization of Biomass: For the Production of Graphite Materials," Stockholm, 2021.

[23] D. M. Stefanescu, T. Tokarski, G. Alonso, M. Górny, and R. Suárez, "On the Role of Turbostratic Graphite in the Crystallization of Spheroidal Graphite During the Liquid-to-Solid Transformation," *Metallurgical and Materials Transactions B*, vol. 54, no. 5, pp. 2283–2290, 2023.

[24] H. Khan, A. S. Yerramilli, A. D'Oliveira, T. L. Alford, D. C. Boffito, and G. S. Patience, "Experimental methods in chemical engineering: X-ray diffraction spectroscopy—XRD," *The Canadian Journal of Chemical Engineering*, vol. 98, no. 6, pp. 1255–1266, 2020.

[25] S. Zhang, N. Ukrainczyk, A. Zaoui, and E. Koenders, "Electrical conductivity of geopolymer-graphite composites: Percolation, mesostructure and analytical modeling," *Construction and Building Materials*, vol. 411, p. 134536, 2024.

[26] E. M. Conners, K. Rengasamy, and A. Bose, "Electroactive biofilms: how microbial electron transfer enables bioelectrochemical applications," *Journal of Industrial Microbiology and Biotechnology*, vol. 49, no. 4, Jul. 2022.

[27] L. Xiaowei, R. Jean-Charles, and Y. Suyuan, "Effect of temperature on graphite oxidation behavior," *Nuclear Engineering and Design*, vol. 227, no. 3, pp. 273–280, 2004.